

MIT Open Access Articles

*Real-time Non-contact Millimeter Wave Characterization
of Water-Freezing and Ice-Melting Dynamics*

The MIT Faculty has made this article openly available. **Please share**
how this access benefits you. Your story matters.

Citation: S. Sundaram, S. Sundaram, and P. Woskov, "Real-time Non-contact Millimeter Wave Characterization of Water-Freezing and Ice-Melting Dynamics," *Journal of Infrared, Millimeter and Terahertz Waves*, vol. 30, Apr. 2009, pp. 393-400.

As Published: <http://dx.doi.org/10.1007/s10762-008-9457-3>

Publisher: Springer New York

Persistent URL: <http://hdl.handle.net/1721.1/49484>

Version: Final published version: final published article, as it appeared in a journal, conference proceedings, or other formally published context

Terms of use: Article is made available in accordance with the publisher's policy and may be subject to US copyright law. Please refer to the publisher's site for terms of use.



Real-time Non-contact Millimeter Wave Characterization of Water-Freezing and Ice-Melting Dynamics

Sudhandra Sundaram · S. K. Sundaram · Paul P. Woskov

Abstract We applied millimeter wave radiometry for the first time to monitor water-freezing and ice-melting dynamics in real-time non-contact. The measurements were completed at a frequency of 137 GHz. Small amounts (about 2 mL) of freshwater or saltwater were frozen over a Peltier cooler and the freezing and melting sequence was recorded. Saltwater was prepared in the laboratory that contained 3.5% of table salt to simulate the ocean water. The dynamics of freezing-melting was observed by measuring the millimeter wave temperature as well as the changes in the ice or water surface reflectivity and position. This was repeated using large amounts of freshwater and saltwater (800 mL) mimicking glaciers. Millimeter wave surface level fluctuations indicated as the top surface melted, the light ice below floated up indicating lower surface temperature until the ice completely melted. Our results are useful for remote sensing and tracking temperature for potentially large-scale environmental applications, e.g., global warming.

Keywords Millimeter wave reflectivity · freezing · melting · fresh/sea water · remote sensing · global warming

S. Sundaram
Phillips Academy
Andover, MA 01810, USA
E-mail: ssundaram@andover.edu

S. K. Sundaram
Pacific Northwest National Laboratory
Richland, WA 99352, USA

P. P. Woskov
Plasma Science and Fusion Center, Massachusetts Institute of Technology
Cambridge, MA 02139, USA

1 Introduction

The dielectric properties (real (ϵ') and imaginary (ϵ'') permittivity) of ice and water have been extensively studied for cloud measurements and geophysical features advancing environmental and atmospheric sciences [1-5]. Recently, an empirical model [6] based on the parameterizations in Liebe et al. [7] and Hufford [8] (called the LH model) was developed using empirical fits to published experimental data at frequencies < 1000 GHz for both ice and water, and limited to temperatures ≥ 0 °C for water. Laboratory measurements of the dielectric properties have been made and published by a number of researchers at millimeter and sub-millimeter wavelengths (~ 100 – 3000 GHz). Accurate measurement of the complex dielectric permittivity, $\epsilon = \epsilon' + i\epsilon''$, of ice and water at these frequencies are critical for using radar in these areas of application.

The scattering of millimeter waves due to melting ice spheres and melting have been treated by many researchers [9, 10]. Maya et al [11] have shown that the monitoring of the water of the leaf of the plant can monitor the aspect of the photosynthesis activity in real-time. They have also monitored the freezing process of the water in the refrigerator and the phase transition of water and ice. Recently, melting snow particles has been modeled by three-layered spherical particles [12], in which the innermost layer is air, the middle ice and the outermost water. Based on this model, the radar reflectivity, together with the specific phase shift and the specific attenuation of a melting layer of precipitation, have been computed at 1–100 GHz by using Mie theory.

Ice on the external fuel tank on the space shuttle can be detrimental to its launch. Millimeter radiometry has been used to measure ice thickness on the space shuttle's external tank [13]. A Spray-On Foam Insulation (SOFI) layer covers the outside of the fuel tank that provides thermal insulation between the aluminum surface of the tank and the ambient air. Model calculations and measurements of the emission properties from an external fuel tank panel were carried out at 35, 94 and 140 GHz. The results demonstrated that the ice thickness on the SOFI panel could be accurately predicted. Recently, a compact millimeter wave system has been developed for deicing and/or preventing the formation of ice on the outer surface of hollow shell structures that are exposed to meteorological influences [14]. In the present paper, we demonstrate novel adaptation of active millimeter-wave radiometry for the first time to non-contact real-time monitor water-freezing and ice-melting dynamics.

2 Experimental procedure

The experimental test set up is shown in Figure 1. A 137 GHz millimeter-wave heterodyne receiver was installed on a vertically movable platform above the sample assembly. The receiver noise temperature is approximately 3,000 K double side band (DBS). The intermediate frequency band is 0.2 – 2.0 GHz for a DBS bandwidth of 3.0 GHz. For a one second integration time this would correspond to a theoretical temperature resolution of 0.05°C. The receiver field-of-view was directed through a horizontal 2.9 cm internal diameter, 46 cm long corrugated brass waveguide (horizontal portion) with a stainless steel miter bend mirror and 7.6 cm long aluminum corrugated vertical section that extended vertically down toward the center of the ice sample/water pool. For the experiments described here, the waveguide end was positioned about 2.5 cm (1 in.) above the sample surface. Figure shows the assemblies for the thin film as well as ice block measurements.

The receiver detected two signals in separate channels; the reflected leaked 137 GHz local oscillator (LO) signal and a 3 GHz wide double sideband (135-136.5 GHz and 137.5-139 GHz) thermal emission signal. The phase of the coherent LO reflection depends on the path length between the receiver and melt surface. Consequently, the reflection signal level when heterodyned with the receiver LO varied between a maximum (in phase) and minimum (out of phase) for every $1/4\lambda$ (0.55 mm) change in the relative distance between the receiver and ice/water surface. Thus, vertical ice/water surface movements were observed with submillimeter precision.

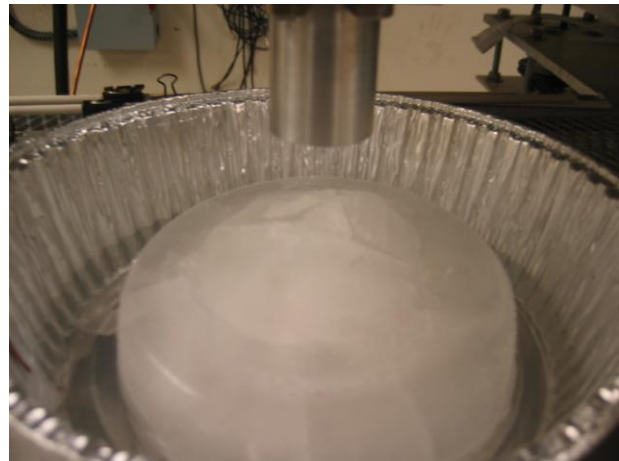
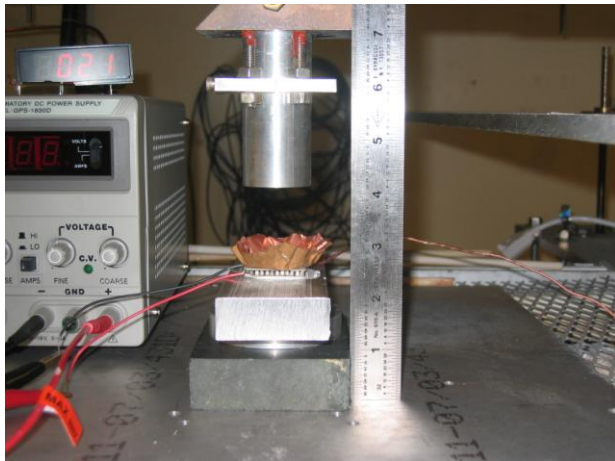
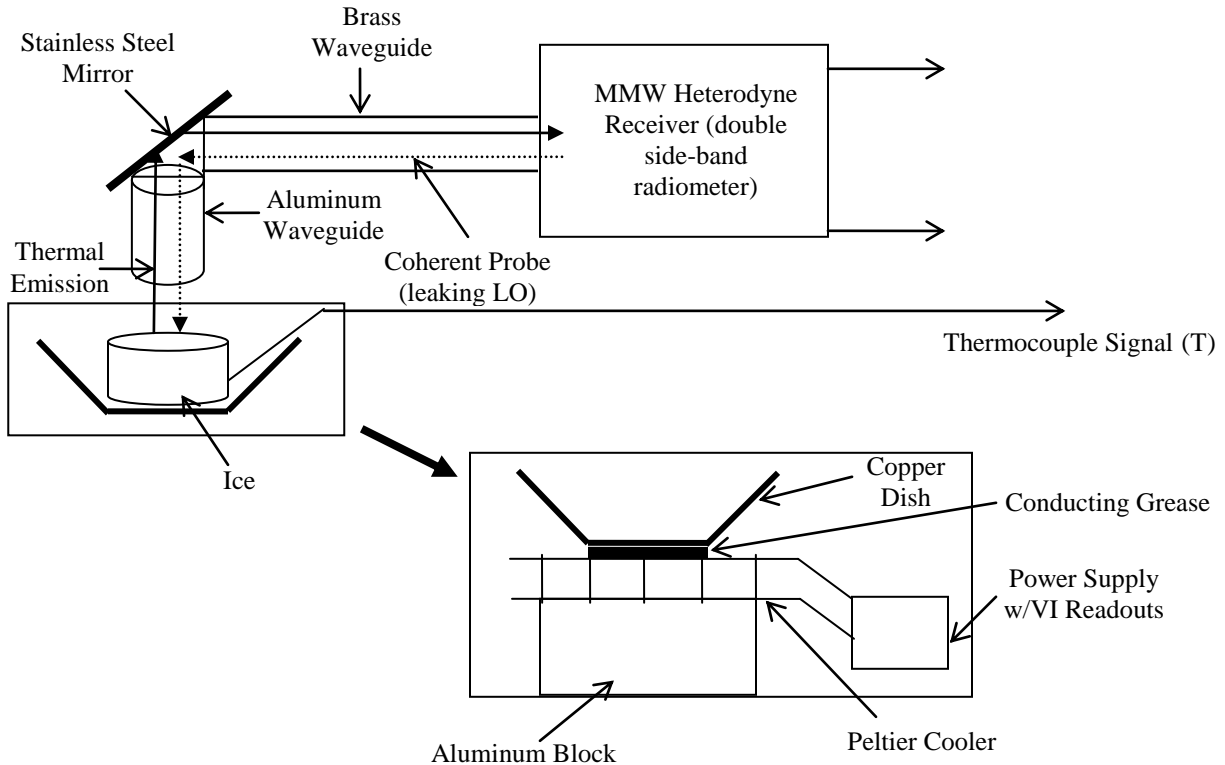


Fig. 1 Top: Schematic of the Experimental Setup; Bottom (left): Fresh Water Thin Film Assembly; Bottom (right): Salt Water Ice Block on a Tray

Temperature and emissivity information were obtained from the broadband MMW thermal signal that is proportional to the product of emissivity and temperature (ϵT). At constant temperature and ice/water surface, changes in the MMW thermal signal provide an indication of changes in emissivity. Since ice and water have significantly different MMW emissivities, the MMW thermal signal provided a clear response to the freezing of water and melting of water below the waveguide view. We took thermal return reflection (TRR) [15] measurements to obtain a quantitative measure of the surface emissivity. In the TRR method, a beamsplitter at the receiver redirects a portion of the thermal signal back to the melt as a probe of its reflectivity. The resulting increase in thermal signal depends on the emissivity (ϵ) and surface figure for coupling (τ_k) the radiation back to the receiver, where the surface figure depends on the surface roughness, curvature, and alignment. This enables capturing the dynamics of water freezing and ice melting.

We used fresh (distilled) water as well as simulated seawater in our testing. Seawater chemistry is a complex area of study. 96.5 % of seawater is indeed water, but the other 3.5 % is salt. The freezing point of fresh water is 0°C , while that of seawater is -1.91°C . We used 3.5% salt to make up salt water mixture for the experiments. We also used 2 mL of water in a 30 mm diameter copper dish for thin film measurements and 800 mL of water in a 152.4 mm diameter aluminum dish for ice block measurements. The thin film was about 2.8 mm thick and the ice block, about 43.9 mm. A Peltier cooler was used to freeze the water for thin film measurements. Large ice blocks were frozen inside a refrigerator first and then transferred to an aluminum pan for the measurements. In the case of ice blocks, we used a ruler to measure the distance between the top of the block to the tip of the wave guide above to determine the thickness of the block as the melting measurements progressed.

A K-type thermocouple in contact with the water and copper dish was used to measure the temperature to compare to the MMW measurements. A thermocouple provides contacted localized temperature readings, while the MMW sensor gives a non contact averaged surface temperature of the viewing area.

3 Results and Discussion

A. Thin Film Freezing-Melting Measurements:

Figure 2 shows one of the three runs done using 2 mL of water in the copper dish. A Peltier Cooler was used to freeze the water with an applied current of about 2.3 A. As the figure depicts, the Peltier voltage was turned on at 60 seconds on the time axis. The MMW temperature (red curve) steadily decreased to about 0°C at 90 seconds when the water completely froze and then at 150 seconds the surface briefly remelted before starting to sharply decrease in temperature again at about 200 seconds. At about 240 seconds the frozen temperature is reestablished and the surface continues to appear frozen until 320 seconds, 70 seconds after the Peltier cooler is turned off. This behavior can be interpreted as follows: The water initially freezes and then due to the different thermodynamic properties of water and ice the surface exposed to the air begins to melt. Being denser, the water flows to the bottom and after the Peltier cooler is turned off the ice melts primarily from the bottom up with the less dense ice floating on the water until it is completely melted. The thermocouple temperature (light green curve) initially followed a similar decrease in temperature as the MMW signal when the Peltier voltage was applied. After about 200 seconds the thermocouple signal deviates from the MMW

signal because it is in contact with the liquid component of the ice/water mixture. This difference between the temperature of the thermocouple and MMW shows that the location of the thermocouple makes a difference in the results. The thermocouple provides localized temperature measurement in contact with the water below the ice while the MMWs provide a surface temperature measurement over a wide viewing area corresponding to the field-of-view of the MMW waveguide. The MMW reflection (black curve) begins to form a fringe at 150 seconds and shows that the sample surface has begun to move (due to the slight surface melting and surface tension). When the Peliter voltage is stopped at 250 seconds, the millimeter wave temperature remains relatively constant until the surface layer of ice disappears, while the thermocouple, in contact with the bottom of the copper dish, shows a steady warm up towards room temperature. The MMW reflection curve shows stability once it reaches the room temperature as at starting point of the experiment (0 second). Though the surface temperature remains same during the experiment, the emissivities for water and ice are different [6]. At 137 GHz the refractive index for water is about 2.65 and that for ice is 1.76. The reflectivity therefore will be different at the surface air boundary and consequently the measured emissivity.

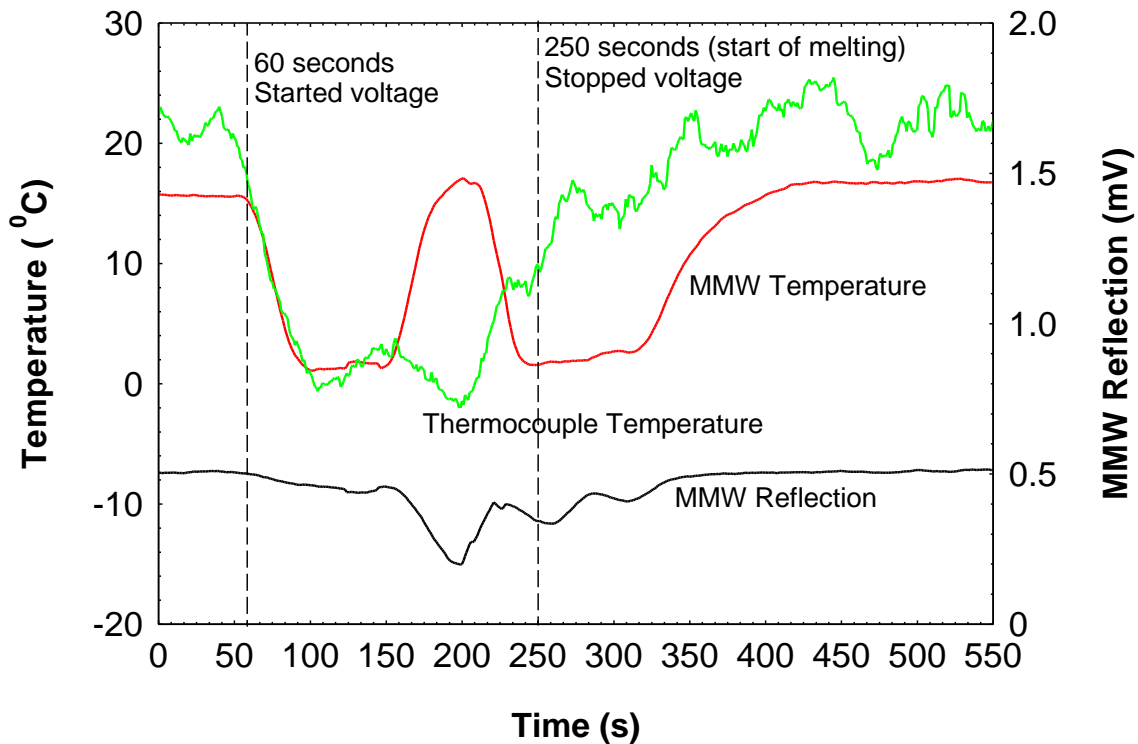


Fig. 2 Freezing/melting dynamics of thin fresh water film

Figure 3 shows that seawater once frozen had its surface temperature stay at the freezing temperature longer (from 100 seconds to 350 seconds) without a surface remelting event while the Peltier cooler was on. However, right after the Peltier cooler was turned off at 250 seconds the MMW reflection signal indicates that a phase transition was occurring even though the surface temperature was not changing significantly. At 275 seconds the reflection signal (black curve) shows a fringe indicating melting of the ice. The surface of the saltwater/ice mixture appears to stay colder longer than the freshwater/ice mixture due to the chemistry change caused by the addition of salt. The MMW and thermocouple temperature measurements illustrate this point from 100 seconds to about 275 seconds. The temperature stays low rather than increase as

seen with the freshwater tests when the MMW waveguide view sensed surface melting after initially freezing. The saltwater ice surface only began rising in temperature about 100 seconds after the voltage was turned off, while the thermocouple in contact with the copper dish shows significant temperature increase began immediately with the Peltier cooler turn off.

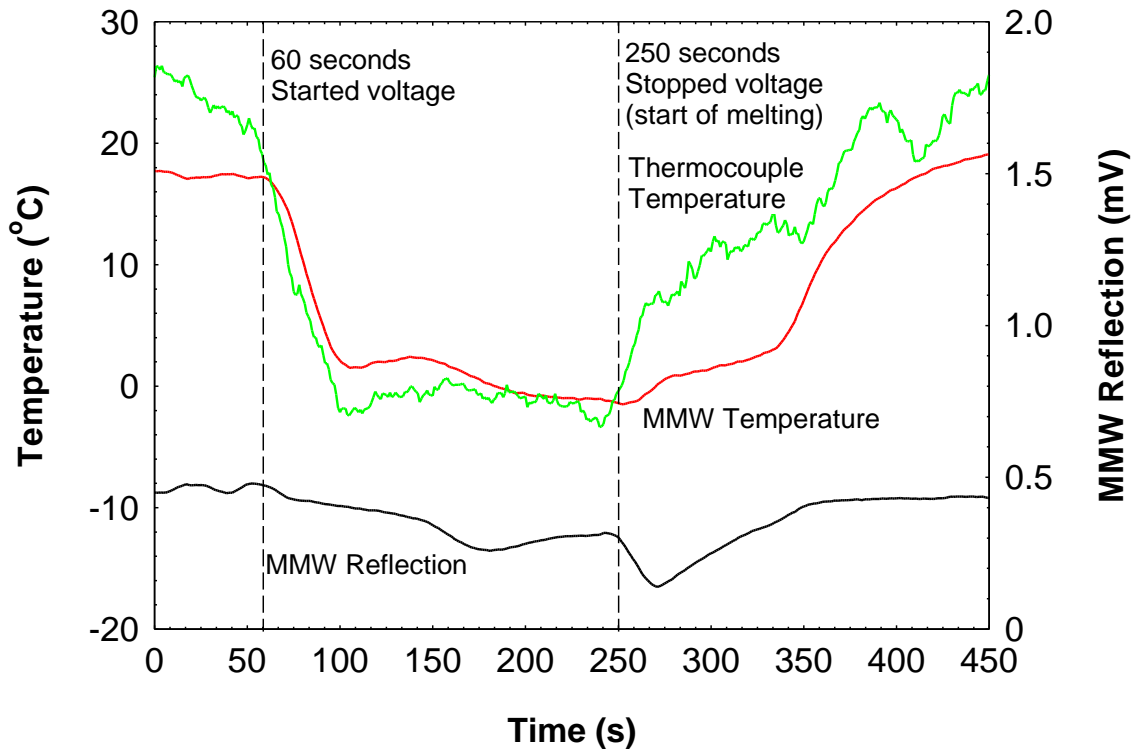


Fig. 3 Freezing/melting dynamics of thin seawater film

B. Large Block Tests:

Figure 4 shows just the melting process of a large block of freshwater (800 mL). It was frozen in a refrigerator for 12 hours. The millimeter-temperature and thermocouple temperature both increased steadily towards room temperature (21°C). The thermocouple does not see the lower temperatures of the ice because it was sensing the temperature of the side of the aluminum pan rather than the ice itself. The millimeter-wave temperature, however, was sensing the exact temperature of the ice (which is less than the pan temperature). This resulted in different starting points for the thermocouple temperature (light green) and the millimeter-wave temperature (red). At around 18000 seconds (5 hours), the temperature began to increase and the ice thus was melting. The difference between the level of the water after melting and the level of the ice after a few seconds created the long fringe from about 20000 seconds to around 65000 seconds. When freshwater ice melts, it contributes a greater volume of melted water (about 9% increase in volume) than it originally displaced. This is due to the difference in density between water (1 g/mL) and freshwater ice (0.92 g/mL). Therefore, the melted water forms a flat surface as the melting proceeds below the surface. Once the melting ends, the melted water level decreases as water is denser than freshwater ice, supporting the long peak observed.

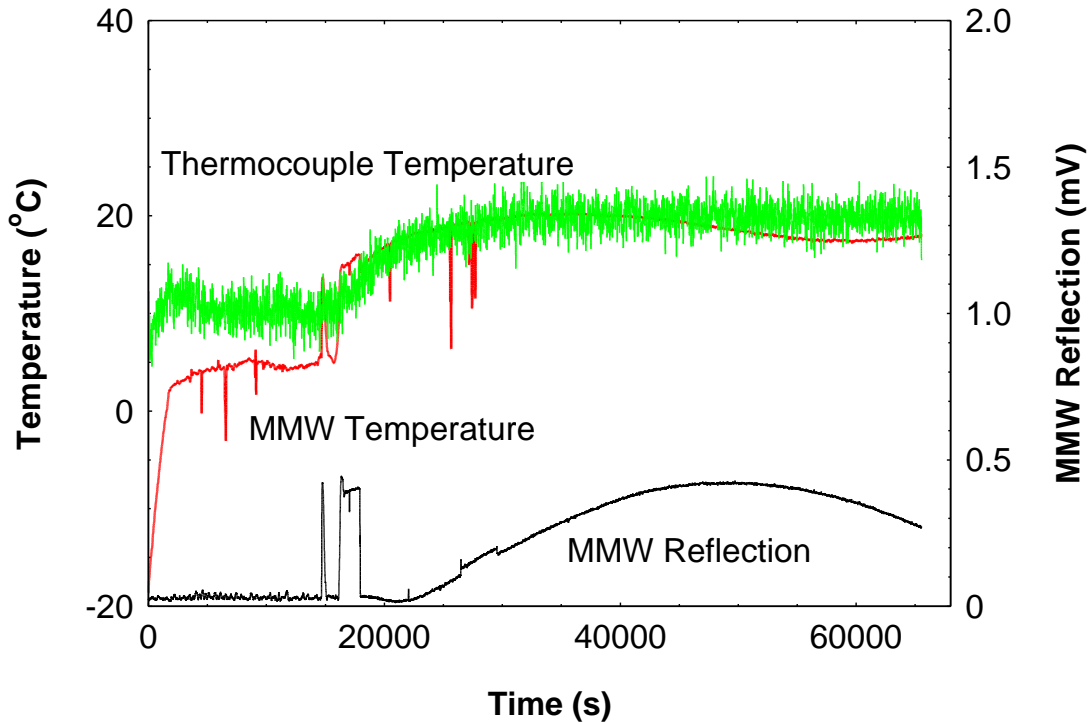


Fig. 4 Fresh Water Block Melting Dynamics

Figure 5 shows the saltwater block during the melting process. The ice clearly started to melt sooner than the freshwater block. There was no stable period initially, rather the melting process started immediately. The MMW reflection (black curve) shows many, rapid fringes. This indicates that the surface was receding rapidly as the ice was melting. The melting started at about 12000 seconds (3-1/3 hours).

It is well-known that adding salt can decrease the freezing temperature of water to as low as -21°C and freshwater is not as dense as saltwater. The density of water is dependent on the dissolved salt content as well as the temperature of the water. Ice still floats in the oceans, otherwise they would freeze from the bottom up. However, the salt content lowers the freezing point by about 2°C and lowers the temperature of the density maximum of water to the freezing point. As the surface of saltwater begins to freeze (at -1.9°C for normal salinity seawater, 3.5%) the ice that forms is essentially salt free with a density approximately equal to that of freshwater ice. This ice floats on the surface and the salt that is "frozen out" adds to the salinity and density of the saltedwater just below it, in a process known as brine rejection. This denser saltwater sinks by convection and the replacing seawater is subject to the same process. This provides essentially freshwater ice at -1.9°C on the surface. The increased density of the seawater beneath the forming ice causes it to sink towards the bottom.

Figure 6 shows the distance between the waveguide and ice block (freshwater and saltwater) in inches. The figure clearly shows that the saltwater block of ice apparently melted faster (thus the distance stabilized to 2.4 at about 2 hours). The freshwater block of ice continued to melt lowering the level gradually up until around the 5th hour. This is mainly attributed to the way MMW temperature is measured (surface measurement).

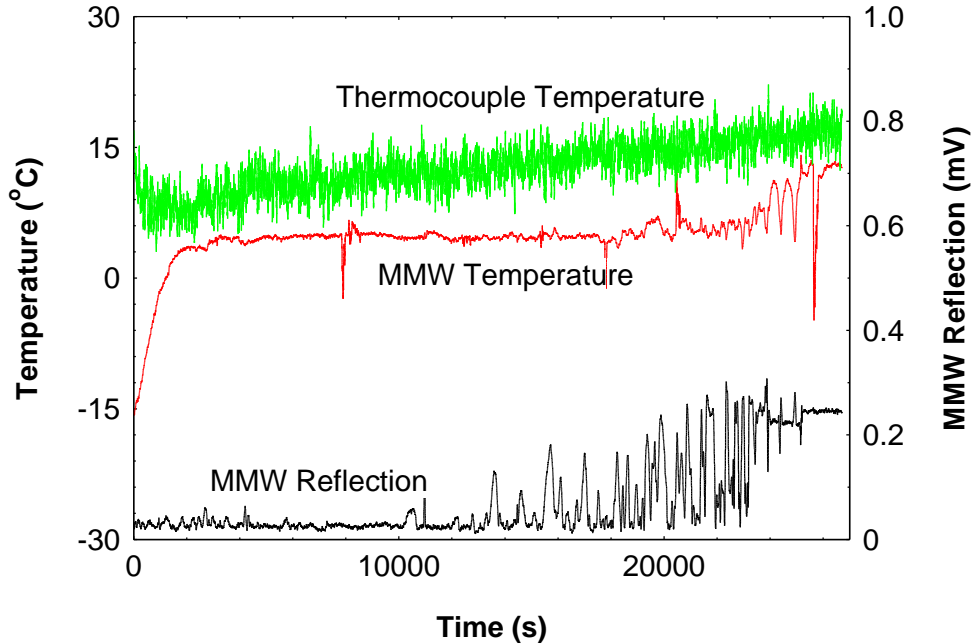


Fig. 5 Salt Water Block Melting Dynamics

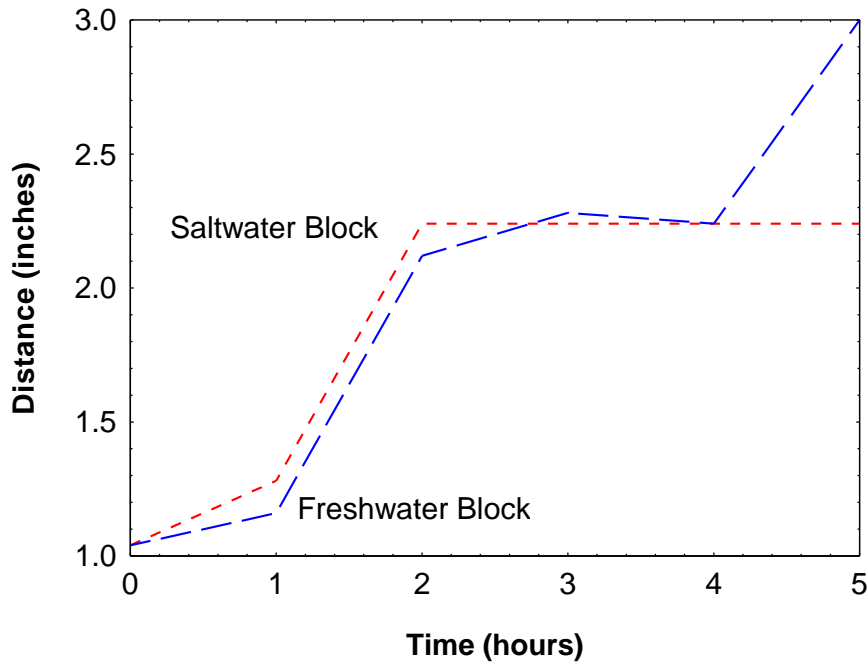


Fig. 6 Fresh Water Block vs. Salt Water Block

4 Conclusion

Our results demonstrate the unique capability of MMWs to monitor the dynamics and changes of water freezing and ice melting non-contact and in real-time. These results show that there are differences between fresh and salt water freezing dynamics that can be observed with active millimeter-wave radiometry. The experiments also demonstrate the scalability of the MMW measurements from thin films of ice to blocks of ice, thus showing promise for

application in remote sensing and measuring temperature and emissivity of different surfaces in the field.

Acknowledgements

SKS acknowledges support from the DOE's Environment Management Science Program (EMSP). Pacific Northwest National Laboratory (PNNL) is a multi-program national laboratory operated by Battelle Memorial Institute for the United States Department of Energy under DE-AC06-76RLO 1830.

References

1. W. A. Cumming, The dielectric properties of ice and snow at 3.2 centimeters, *Journal of Applied Physics* **23**(7), 768–773 (1952)
2. J. Perry and A. W. Straiton, Dielectric constant of ice 35.3 and 94.5 GHz. *Journal of Applied Physics* **43**(2) 731-733 (1972); J. Perry and A. W. Straiton, Revision of dielectric-constant of ice in millimeter-wave spectrum, *Journal of Applied Physics* **44**(11): 5180–5180 (1973)
3. M. R. Vant, R. B. Gray, R. O. Ramseier, and V. Makios, Dielectric properties of fresh and sea ice at 10 and 35 GHz, *Journal of Applied Physics* **45**(11), 4712-4717 (1974)
4. C. Mätzler and U. Wegmüller, Dielectric properties of freshwater ice at microwave frequencies, *Journal of Physics D: Applied Physics* **20**, 1623–1630 (1987)
5. G. Koh, Dielectric properties of ice at millimeter wavelengths, *Geophysical Research Letters* **24**(18), 2311–2313 (1997)
6. J. H. Jiang and D. L. Wu, Ice and water permittivities for millimeter and sub-millimeter remote sensing applications, *Atmos. Sci. Let.* **5**, 146–151 (2004)
7. H. J. Liebe, G. A. Hufford, and T. Manabe, A model for the complex permittivity of water at frequencies below 1 THz, *International Journal of Infrared and Millimeter Waves* **12**(7), 659–674 (1991)
8. G. Hufford, A model for the complex permittivity of ice at frequencies below 1 THz, *International Journal of Infrared Millimeter Waves* **12**(7), 677–682 (1991)
9. T. Oguci, Scattering and absorption of a millimeter wave due to melting ice spheres, *Proc. of the IEEE*, 883-885 (1966)
10. W. Zhang, E. Salonen, and S. Karhu, Calculations of millimeter wave depolarization due to melting layer and rain, *Int. J. Infrared and Milli. Waves*, **12** (5), 543-556 (1991)
11. M. Maya, S. Kenji, O. Yuichi, O. Chiko, and K. Kodo, Monitoring of water content and frozen state by using millimeter wave absorption features, *Transactions of the Institute of Electrical Engineering of Japan. E* **125**(5), 229-233 (2005)
12. X. Sun, H. Wang, Y. Han, and X. Shi, A new melting particle model and its application to scattering of radiowaves by a melting layer of precipitation, *Int. J. Infrared and Milli. Waves*, **28**, 993-1001 (2007)
13. J. E. Kendra1, F. T. Ulaby, and S. Wu, A millimeter wave technique for measuring ice thickness on the Space Shuttle's external tank, *Int. J. Infrared and Milli. Waves*, **12** (12), 1349-1377 (1991)
14. L. Feher, Compact millimeter wave technical system for deicing and/or preventing the formation of ice on the outer surface of hollow or shell structures exposed to meteorological influences, European patent EP1284903, Published on 02/26/2003.

15. P. P. Woskov and S. K. Sundaram, Thermal return reflection method for resolving emissivity and temperature in radiometric measurements, *J. Appl. Phys.* **92**(10), 6302- 6310 (2002)